Nanoscale

RSC Publishing

PAPER

Dynamic templating: a large area processing route for the assembly of periodic arrays of sub-micrometer and nanoscale structures†

Cite this: *Nanoscale*, 2013, **5**, 1929

Pouyan Farzinpour, Aarthi Sundar, Kyle D. Gilroy, Zachary E. Eskin, Robert A. Hughes* and Svetlana Neretina*

A substrate-based templated assembly route has been devised which offers large-area, high-throughput capabilities for the fabrication of periodic arrays of sub-micrometer and nanometer-scale structures. The approach overcomes a significant technological barrier to the widespread use of substrate-based templated assembly by eliminating the need for periodic templates having nanoscale features. Instead, it relies upon the use of a dynamic template with dimensions that evolve in time from easily fabricated micrometer dimensions to those on the nanoscale as the assembly process proceeds. The dynamic template consists of a pedestal of a sacrificial material, typically antimony, upon which an ultrathin layer of a second material is deposited. When heated, antimony sublimation results in a continuous reduction in template size where the motion of the sublimation fronts direct the diffusion of atoms of the second material to a predetermined location. The route has broad applicability, having already produced periodic arrays of gold, silver, copper, platinum, nickel, cobalt, germanium and Au–Ag alloys on substrates as diverse as silicon, sapphire, silicon–carbide, graphene and glass. Requiring only modest levels of instrumentation, the process provides an enabling route for any reasonably equipped researcher to fabricate periodic arrays that would otherwise require advanced fabrication facilities.

Received 8th December 2012
Accepted 14th January 2013

DOI: 10.1039/c3nr33992k

www.rsc.org/nanoscale

Introduction

At the cornerstone of the electronics industry is a processing science dedicated to the fabrication of wafer-based materials and interfaces with well-defined properties situated at well-defined locations. This industry is now facing the challenges associated with defining features on nanometer length-scales. Meeting these challenges will enable a broad range of potential applications with a scope that includes biological,[1,2] chemical[3,4] and light sensors,[5] photovoltaics,[6] plasmonics,[7] nanoscale electronics,[8] magnetic memory,[9] metamaterials,[10] catalysis,[11] and applications based on seeded nanowires.[12] Photolithographic techniques, which have been the mainstay of the semiconductor industry, are responding to these challenges through the introduction of increasingly sophisticated techniques which include 193 nm immersion lithography,[13] extreme ultraviolet lithography,[14] interference lithography,[15] and step and flash imprint lithography.[16] Associated with these advanced techniques are technological and economic barriers which limit their access to all but the most-sophisticated fabrication facilities. In response to these technically demanding cost-prohibitive routes has been the development of a multitude of unconventional lithographic techniques focused on the formation of patterned photoresist materials.[17–20] While far less cost-prohibitive, each of these routes faces their own distinctive technological hurdles. Other unconventional routes avoid the use of photoresist materials, instead opting for the use of nanoscale apertures (*e.g.* nanosphere lithography,[21] stencil lithography[22,23]) or the direct imprinting of metallic structures.[24,25] These techniques, while yielding impressive results, have not yet demonstrated the scalability and high-throughput characteristics needed for wafer-scale integration. In contrast, low-cost self-assembly processes have proved quite effective in the formation of substrate-supported nanostructures with arbitrarily small dimensions, but where their accurate placement has proved exceedingly dificult. Notable procedures giving rise to the near-random formation of nanostructures on substrate surfaces include thermal dewetting,[26] vapour phase epitaxy,[27] the linking of solution-formed nanostructures,[28] spinodal dewetting,[29] and microwave plasma-induced dewetting.[30] Among these, the thermal dewetting of ultrathin continuous films stands out as both cost-effective and, from a technical standpoint, straightforward.

College of Engineering, Temple University, Philadelphia, PA, USA. E-mail: neretina@temple.edu; hughesr@temple.edu; Fax: +1 215 204 4956; Tel: +1 215 204 6326

† Electronic supplementary information (ESI) available: Provided are additional figures showing a compilation of SEM images of gold arrays deposited on various substrates using dynamic templating, SEM and Raman spectra of graphene after a periodic gold array has been assembled on its surface, DDA simulations of the plasmonic response of gold nanoparticles, a histogram displaying array registration errors and a table listing growth parameters. See DOI: 10.1039/c3nr33992k

The deposition of a high surface energy thin film on a low surface energy substrate, followed by its subsequent dewetting and agglomeration into droplets at elevated temperatures, is the most straightforward method for obtaining substrate-based nanostructures. The mechanisms governing this dewetting phenomenon, however, are quite complex and are influenced by the film thickness,[31] the crystallographic orientation of the substrate[32] and film,[33] substrate surface reconstructions,[27] the substrate–film lattice mismatch,[32] faceting,[34] and interface chemistry.[35] This multitude of factors leads to limited control over and a randomness in the nanoparticle size distribution, spacing and placement. The imposition of a periodicity onto the dewetting process using lithographically defined film edges,[31,33,36–39] periodic templates[31,40] or substrate surface texture[41–43] has been demonstrated. To carry out these so-called templated dewetting procedures on the nanoscale, however, requires that order be imposed by patterns having nanoscale features. For example, when a film is deposited on a substrate and subsequently patterned to form a square with width 'w' and thickness 'h', there exists a pattern-width-to-film-thickness ratio (*i.e.* w/h) below which it is able to agglomerate into a single structure when heated and above which it breaks up into multiple structures. This ratio is, under ideal circumstances, often below 100.[44] Calculations based on this value reveal that pattern widths of less than 200 nm are typically required for the agglomeration of 50 nm nanostructures. Producing periodic templated structures on these length-scales over large areas in a manner which preserves long range order becomes technically challenging and cost-prohibitive, negating the main advantage of using the templated dewetting route. An alternative approach uses easily fabricated micrometer-scale templates to produce an array of larger structures which are subsequently reduced in size through the use of surface energy gradients[45] or high temperature anneals.[31] Maintaining control over the process, however, becomes increasingly challenging as the nanoparticle length-scale is reduced. Here, we report on an assembly route, referred to as dynamic templating, which yields w/h ratios two orders of magnitude higher than that observed for conventional dewetting techniques. The discovery enables the templated assembly of nanostructured arrays using templates having easily manufactured micrometer-scale features.

Results

The processing route used to fabricate periodic arrays of sub-micrometer and nanometer-scale gold structures is shown schematically in Fig. 1a. A shadow mask consisting of a periodic array of openings is placed over the substrate. Deposited through this mask onto the substrate is a thicker sacrificial layer followed by a second ultrathin gold layer which ultimately assembles to form the gold structures. Room temperature gold films typically show a surface texture on nanoscale length-scales and, from the standpoint of the current study, are most aptly described as quasi-continuous. Antimony was chosen as the sacrificial layer because it readily sublimates in the temperature regime where gold films typically dewet and it has a much lower surface energy than gold,[46] an attribute which promotes gold agglomeration. The shadow mask is then removed and the remaining layered structure is heated to temperatures amenable to dewetting. In contrast to conventional templated dewetting, where the gold structure is formed on a substrate material, the gold must now agglomerate upon a sacrificial antimony pedestal which is simultaneously being annihilated as antimony atoms leave the structure through sublimation. This reduction in pedestal area results in a forced migration of the agglomerating gold atoms to the center of the structure. Once all the antimony is driven from the substrate surface through sublimation, a single gold structure is left in the center. The terminology "dynamic template" has been adopted to describe the shrinking antimony pedestal. It is used to contrast its dynamic nature with the passive templates used in conventional templated assembly. The nomenclature of passive and dynamic templating will, hence, refer to the conventional and newly devised fabrication route, respectively, but where it should be recognized that the devised route combines both passive (*i.e.* the shadow mask) and dynamic templating.

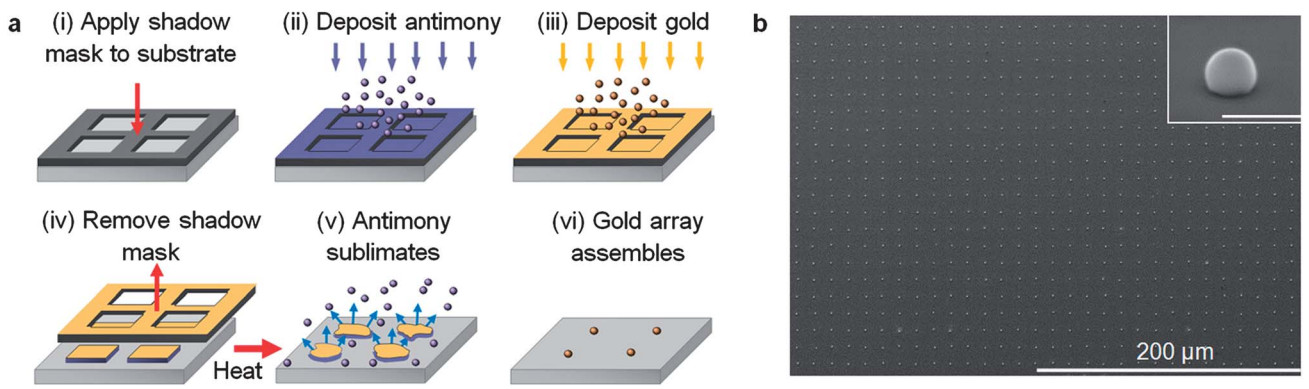

Fig. 1 (a) A schematic of the dynamic templating process used to assemble periodic arrays of sub-micrometer and nanometer-scale gold structures. The process proceeds by (i) applying a shadow mask to the substrate, (ii) depositing antimony through the mask to form the dynamic template, (iii) depositing the gold onto the dynamic template, (iv) removal of the shadow mask, and then (v) heating the sample to induce both gold agglomeration and antimony sublimation until (vi) only a periodic array of gold structures remain. (b) An SEM image of a large-area array of sub-micrometer gold structures produced using dynamic templating on a (0001)-oriented sapphire substrate. The inset is a high magnification image of an individual gold structure presented from a 65° tilt side-view (scale bar = 1 μm).

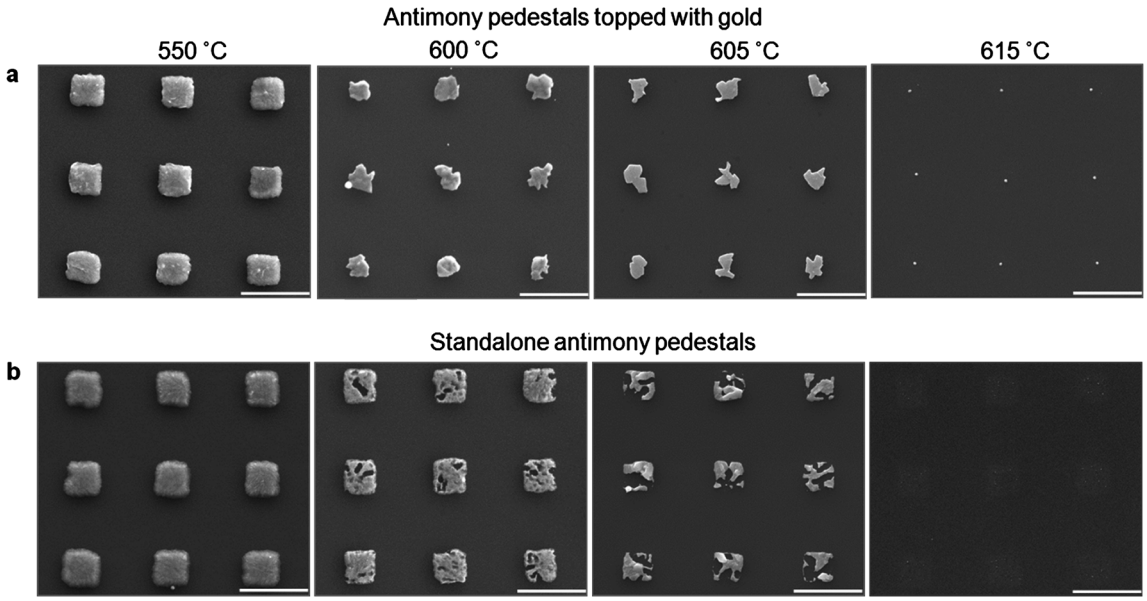

Fig. 2 SEM images showing the evolution of (a) 5 μm × 5 μm × 200 nm antimony pedestals topped with 0.25 nm of gold (*i.e.* dynamic templating) formed on (0001)-oriented sapphire substrates and (b) identical standalone antimony pedestals as they are heated to various temperatures and then quenched. Note that as the antimony sublimates the gold-topped pedestals retract from the edges defined by the shadow mask while the standalone pedestals break-up prior to complete annihilation through sublimation. It is noted that the arrayed structures imaged at 615 °C are still antimony-rich (55 wt% Sb), but where further heating drives away the remaining antimony. The scale bar is 10 μm.

Dynamic templating has been used to fabricate large-area arrays such as the one shown in Fig. 1b.

Fig. 2a shows SEM images obtained from a series of samples where the dynamic templating process was interrupted at various stages by heating and then quenching gold-topped antimony pedestals from progressively higher temperatures. In all cases, the maximum temperature was below the melting point of antimony ($T_m = 630.8$ °C). This series is contrasted with standalone antimony pedestals quenched from the identical temperatures (Fig. 2b). Immediately evident is that the standalone pedestals retain their original areal dimensions as they sublimate, break-up and ultimately disappear from the substrate surface. This behaviour is consistent with antimony having a surface energy that is lower than the underlying substrate and where sublimation is primarily through the loss of atoms from the top surface of the pedestal due to its much higher surface area. In contrast, the dynamic templating process is characterized by well-defined edges which retract in an organized manner as they diminish in size from the original pedestal structure to a single near-hemispherical gold nanostructure. For this case, gold inhibits the loss of antimony from the top of the pedestal, the result of which is a sublimation process dominated by the loss of atoms from the pedestal sides.

Fig. 3 shows a comparison of the results obtained when using passive and dynamic templating for gold films of two different thicknesses (5 and 0.5 nm) where each was exposed to the same heating regimen. For the 5 nm case, passive templating yields as many as 40 nanoparticles per cell, while dynamic templating yields a single near-hemispherical gold structure (radius = 385 nm) in the center of each cell having a volume equal to the combined volume of the smaller nanoparticles. For the 0.5 nm thick sample the difference is even more striking, showing nearly negligible agglomeration for passive templating while, once again, showing a single

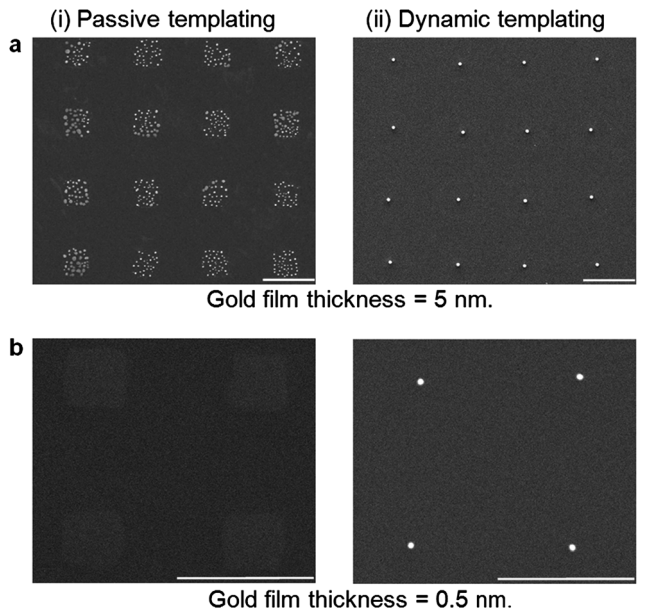

Fig. 3 A comparison showing the advantage of dynamic templating over conventional passive templated dewetting for structures formed on (0001)-oriented sapphire substrates. The SEM images show the degree of agglomeration obtained using (i) conventional passive templating and (ii) dynamic templating for gold film thicknesses of (a) 5 nm and (b) 0.5 nm. Note that dynamic templating yields an array of gold particles while passive templating has only limited influence on the agglomeration process since film dewetting occurs on much smaller length-scales than those defined by the template. The scale bar is 10 μm.

hemispherical nanoparticle per cell (radius = 175 nm) for the dynamic template. The result demonstrates that the dynamic template can support dewetting into a single structure for w/h ratios as large as 10 000 (*i.e.* a 5 μm pattern width divided by a 0.5 nm gold film thickness). Passive templating, on the other hand, is limited to ratio values of approximately 50 for the gold patterns deposited on sapphire. Herein lies the most important advantage of dynamic templating: it enhances the dewetting to the extent that easily manufactured shadow masks, having micrometer-scale features, can yield periodic arrays of nanoscale structures. This is in stark contrast to conventional templating techniques where nanoscale

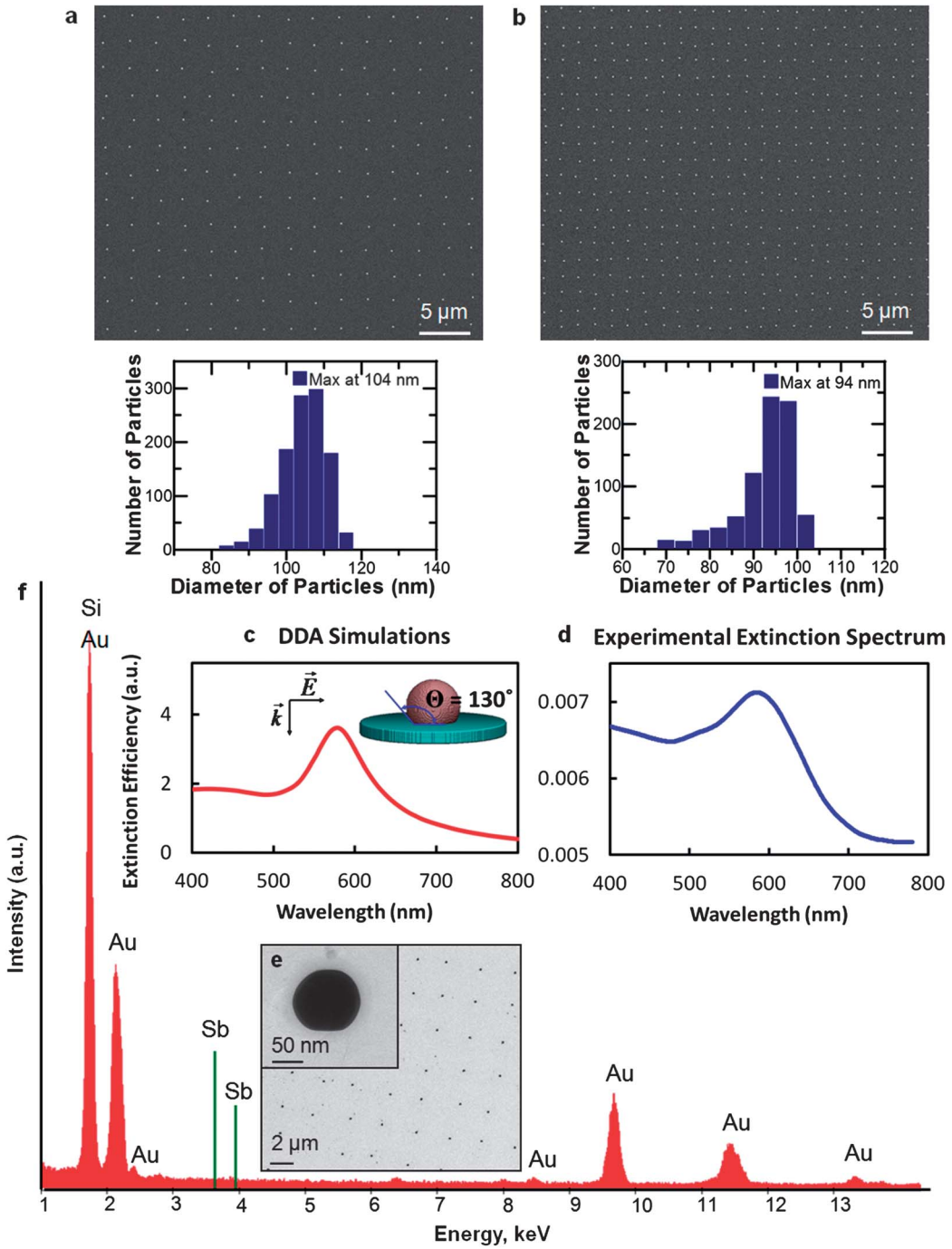

Fig. 4 SEM images and the resulting size distributions of dense arrays of gold nanostructures fabricated on (0001)-oriented sapphire using shadow masks with (a) 1.2 μm diameter openings and a center-to-center distance of 2.6 μm and (b) 0.6 μm diameter openings and a center-to-center distance of 1.6 μm. (c) The extinction spectrum of the arrayed structures shown in (a) and (d) the calculated response based on DDA simulations of a 110 nm diameter gold nanoparticle sharing a contact angle of 130° with a sapphire substrate (inset). (e) Image of a gold array which was similarly fabricated directly on a silicon nitride TEM membrane and (f) the corresponding energy dispersive spectroscopy (EDS) spectrum of an individual nanostructure which shows peaks corresponding only to gold and the underlying Si_3N_4 membrane. Note that there is no signature in the EDS measurement corresponding to antimony.

structures are only formed when the template has nano-scale features.[47]

While conventional dewetting is highly dependent on the substrate material, dynamic templating is not. This is not surprising since the substrate only comes into play in the latter stages of the assembly process when the antimony is nearly depleted. Arrays of gold structures have been fabricated on a wide variety of substrate materials including sapphire, $SrTiO_3$, MgO, YSZ, $MgAl_2O_4$, SiC, fused silica, glass (Eagle XG) and silicon with either a native oxide or 100 nm SiO_2 layer (ESI Fig. S1†). It has been demonstrated on amorphous surfaces, the (0001)-surface of hexagonal crystals and the (001)-, (110)- and (111)-surfaces of cubic crystals. Even substrate-supported monolayer graphene resulted in the formation of gold arrays, but where the SEM images showed some darkening at the locations occupied by the antimony pedestal prior to its sublimation (ESI Fig. S2a†). Raman measurements on these areas reveal the characteristic G- and 2D-bands of single layer graphene as well as the D-band associated with defects[48] (ESI Fig. S2b†). When gold is dewetted directly on graphene the 2D-band is absent due to the severe degradation in the lattice structure.[5]

While shadow masks with 5 μm × 5 μm square openings and 12 μm center-to-center distances between openings were used to demonstrate the enhanced dewetting characteristics available through dynamic templating, the low density of the resulting structures is unsatisfactory for most applications. The collective optical response from the ensemble of such nanostructures is also quite weak. From both these standpoints, dynamic templating is a far more effective processing route when shadow masks with smaller openings and closer center-to-center distances are used. This also allows for the use of antimony pedestals with significantly reduced heights. Fig. 4a and b demonstrate this capability showing periodic arrays of gold nanostructures with a 21-fold and 56-fold increase in particle density (1.5×10^7 cm^{-2} and 3.9×10^7 cm^{-2}). They were fabricated using shadow masks with 1.2 μm and 0.6 μm diameter round openings and center-to-center distances of 2.6 μm and 1.6 μm, respectively. The arrays exhibit narrow size distributions with approximately 90% of the structures falling within ±10 nm of the histogram maximum. The structures shown in Fig. 4a show a plasmon resonance centered at a wavelength of 590 nm (Fig. 4c), a value in agreement with simulations based on the discrete dipole approximation (DDA)[49,50] (Fig. 4d and ESI Fig. S3†). Arrays similar to that shown in Fig. 4a were also fabricated directly on silicon nitride TEM membranes. The individual nanostructures observed show some faceting (Fig. 4e) with no evidence of antimony contamination (Fig. 4f). It is noted that the array quality is somewhat diminished when fabricated directly on these grids because it is difficult to create conformal contact between the grid and shadow mask.

Regardless of the shadow mask size, dynamic templating rapidly loses its effectiveness when the gold film thickness is reduced to values below a monolayer. For this case multiple structures per pedestal are formed. This effectiveness, however, is restored by creating a two-layer template consisting of an antimony pedestal topped with 4 nm of silver, an element which is also prone to sublimation at elevated temperatures. For this case, the assembly occurs in two stages, a first stage where the gold and silver agglomerate together as the antimony pedestal sublimates and a second stage where silver sublimates as the gold continues to agglomerate. The resulting enhancement to the agglomeration process is so extraordinary that it is now possible to accumulate in a predetermined location a mere 700 000 atoms scattered over a 25 μm^2 area into a nanoparticle with a height of 19 nm (Fig. 5). Assuming that such a structure has a hemispherical geometry, then the overall assembly process is characterized by a 600 000-fold volume reduction between the initial pedestal and the final nanostructure. For passive templating to achieve the same degree of success, a film thickness of 1/500th of a monolayer deposited over the same area would have to agglomerate into a single nanostructure, a scenario which is of infinitesimal probability. The assembly process is remarkable in that gold atoms which, from the standpoint of Coulombic interactions, are initially isolated from one another (average area occupied per gold atom = 36 nm^2) are brought together to form a single nanostructure. Drawbacks to this Ag–Sb multilayer pedestal approach include the possibility of silver contamination and the need for higher processing temperatures (930 °C) to induce silver sublimation from the nanostructure.

Even though the main focus of this report is the assembly of gold structures using the dynamic templating approach, it is noteworthy that the process has been applied to a wide variety of material systems. It has, thus far, proved successful in the formation of periodic arrays of gold, silver, copper, platinum, nickel, cobalt, germanium and Au–Ag alloys (Fig. 6). These investigations not only demonstrate the broad applicability of the approach, but also reveal fundamental insights into the mechanisms guiding the assembly process. For all of the aforementioned elements, the use of an antimony pedestal resulted in an enhancement to the dewetting when compared to the bare substrate. The enhancement, however, was much stronger for those elements which form a low temperature eutectic with antimony (Au, Ag, and Ge). Array formation for the other elements using 5 μm × 5 μm shadow mask openings required the use of bismuth instead of antimony as a pedestal material. In this case, the bismuth pedestal is liquid (T_m = 271.4 °C) at

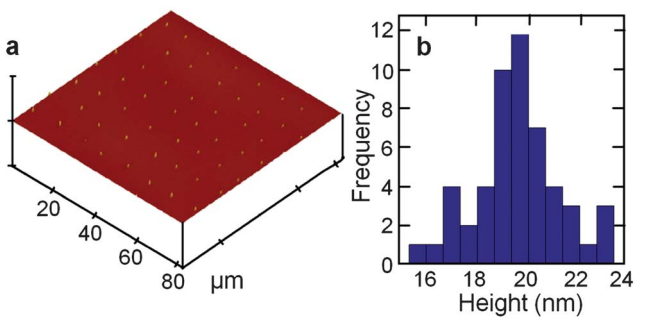

Fig. 5 (a) Atomic force microscopy (AFM) image of an array of gold nanostructures fabricated using a two-layer dynamic template and (b) the associated histogram of the nanostructure heights derived from cross-sections performed on each structure. The substrate used is (100)-oriented $MgAl_2O_4$.

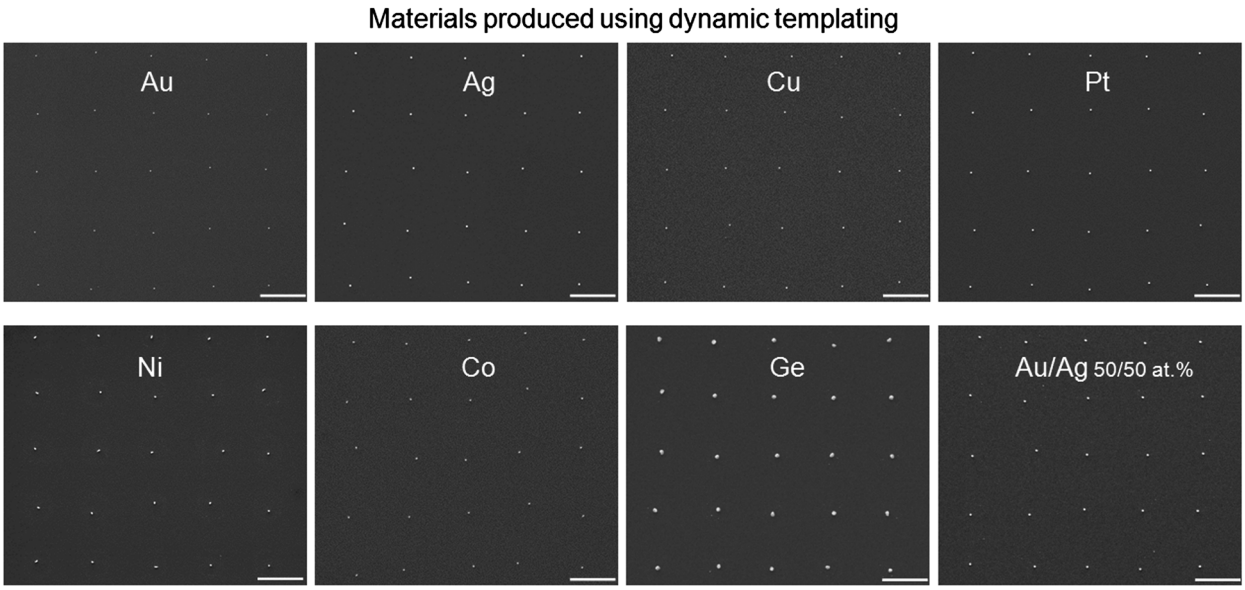

Fig. 6 A compilation of SEM images demonstrating the ability of dynamic templating to fabricate arrays of numerous elements and alloys on (0001)-oriented sapphire substrates. The scale bar is 10 μm.

temperatures where the assembly occurs and where its annihilation is through the process of evaporation rather than sublimation. Bismuth pedestals, while superior in many respects, have the disadvantages that they: (i) show a greater tendency for leaving much smaller nanostructures adjacent to those forming the array, (ii) left the surfaces of some substrates scarred at the pedestal locations and (ii) required faster processing times to achieve optimal results. These disadvantages were, to a large extent, negated through the use of a pedestal consisting of antimony topped with a thin layer of bismuth. The use of antimony, however, was impossible when forming nickel arrays due to high levels of antimony remaining in the assembled structures (10 at%). Some of the arrayed silver structures also had detectable levels of antimony. Palladium arrays showed the highest levels of antimony contamination (30 at%).

Discussion

As a substrate-based directed assembly route, dynamic templating is unique in its ability to assemble nanometer-thick layers spread out over square-micrometer areas into a single structure. It is lithography-free, straightforward, inexpensive, requires only modest levels of instrumentation and can be carried out in several hours. Numerous material systems are accessible and the assembly is supported by a wide variety of substrates. The process also promotes a high degree of crystallinity, where opportunities exist in terms of fabricating arrays of highly faceted three-dimensional structures forming a heteroepitaxial relationship with the underlying substrate. Another important advantage of the technique is that a single shadow mask can be used to assemble structures with widely varying sizes by merely altering the amount of material deposited atop the pedestal. The assembly process does, however, have its shortcomings. A histogram plotting the distribution of the four nearest-neighbor nanoparticle distances for 440 arrayed structures reveals that deviations of hundreds of nanometers from the expected periodicity of 2.6 μm are common (ESI Fig. S4†). While the ability to assemble material from large areas greatly simplifies the array fabrication process, it also places limitations on array pitch. Arrays utilizing micrometer-scale shadow mask openings are restricted to pitch values having the same micrometer length-scale. A final limitation is that the assembly process is more prone to the incorporation of impurities into the final structure. This limitation originates from the high temperatures used in the processing route and the fact that the final assembled structure evolved from a sublimating pedestal with a much larger volume. This volume inevitably contains impurities which can become incorporated into the assembly process.

The mechanisms driving dynamic templating are highly complex, involving a layered structure which emits material, intermixes, evolves from micrometer to nanoscale dimensions and where constituents undergo multiple non-equilibrium phase transitions between the solid, liquid and vapour phases. Nevertheless, key requirements for the process have emerged: (i) the rapid loss of material from the pedestal through sublimation (or evaporation), (ii) the preferential loss of this material from the pedestal sides due to the inhibition of the sublimation process (or evaporation) by material atop the pedestal and (iii) the formation of a liquid at the interface between the pedestal and the agglomerating material. It is important to note that, while the initial choice of antimony as the pedestal material was based on its low surface energy and propensity for sublimating at temperatures where gold atoms typically agglomerate, the interactions between gold and antimony, as depicted by the Au–Sb binary phase diagram, lead to a far more complex situation. Of specific relevance is the fact that antimony is nearly immiscible in gold in the solid state (0.75 wt% Sb), but forms a eutectic with gold which lowers the melting point to nearly

one-third its bulk value (T_E = 360 °C). Little interdiffusion is, thus, expected across a Au–Sb interface below the eutectic temperature. Above the eutectic temperature significant interdiffusion will occur, a process which ultimately gives rise to a transformation from the solid to liquid phase fields of the binary phase diagram. It should be recognized, however, that that the binary phase diagram presents the equilibrium state; it does not offer information about the time-scales required to reach equilibrium. The situation is further complicated by the fact that antimony can diffuse through the gold layer and subsequently sublimate. The kinetics describing these processes are not documented, but inevitably play an important role in the assembly of the gold arrays.

The early stages of the assembly process sees a temperature rise which leads to the onset of antimony sublimation. From the progressions shown in Fig. 2 it is evident that this sublimation process is influenced greatly by the presence of a gold capping layer. Standalone antimony pedestals sublimate without any significant agglomeration and where material loss is primarily through the top surface of the pedestal. The situation, however, is radically altered by the placement of gold on the pedestal (Fig. 2a) as it severely inhibits the antimony sublimation from the top surface, the result of which is a sublimation process dominated by the loss of atoms from the pedestal sides. The net effect is a highly anisotropic sublimation process which continuously reduces the top surface area of the pedestal. It is this antimony sublimation front which drives gold towards the center of the pedestal.

While the forced agglomeration of gold due to the advancement of the sublimation front represents a key mechanism in the assembly process, it is completely reliant on maintaining a quasi-continuous capping layer which inhibits the sublimation through the pedestal top. The importance of maintaining this capping layer is apparent from the observed deterioration in the dynamic templating process (i) when submonolayer gold thicknesses are used and (ii) when the gold is intermixed with the antimony rather than placing it atop the pedestal. Even though some dissolution of antimony through the gold layer is inevitable, its lifetime on the gold surface will be short in duration due to the high antimony vapour pressure at the assembly temperature ($\approx 10^{-1}$ Torr). It would also be quite detrimental to the assembly process if the capping layer dewet on the top surface of the pedestal before the sublimation front arrived. Opposed to this tendency, however, is the wetting behaviour derived from the formation of the Au–Sb eutectic arising from the dissolution of antimony into the gold layer. Such behaviour, referred to as dissolutive wetting,[51] has been observed both experimentally[51–53] and in simulation[54] in such systems as copper-on-silicon and tin-on-bismuth. We, thus, postulate that the dissolution of the pedestal material into gold is a key mechanistic requirement necessary to maintain the integrity of the capping layer and, hence, enable the enhanced dewetting observed. In this respect, the formation of silver and germanium arrays is analogous to that of gold formation in that dissolution occurs through the formation of a eutectic. For other material systems (Pt, Cu, Ni, Co), where a low-temperature eutectic is not present, the dissolution is facilitated through the use of a thin liquid bismuth layer. This result suggests that other low melting point elements with high vapour pressures (*e.g.* Zn, Cd, Se, Te) could also act as effective pedestal materials.

In the late stages of the assembly process, antimony loss is so severe that the pedestal collapses, yielding a liquid phase antimony-gold structure which makes contact with the underlying substrate material. Continued heating leads to further antimony loss which is followed by the onset of solidification, a transformation which occurs when the antimony content drops below values needed to be in the liquid phase field of the binary phase diagram. This will result in the precipitation of gold from the liquid as antimony continues to leave the structure. The near-immiscibility of gold and antimony renders this transformation relatively straightforward. Eventually the antimony will be exhausted and the gold nanostructure will lie on the surface of the substrate with its contact angle in the equilibrium configuration.

At the end of the assembly process dynamic templating yields arrayed structures which appear identical to those obtained through the conventional approach utilizing passive templates. The key advantage of the dynamic templating approach, however, is that much smaller structures can be assembled from a template of a set width. For the assembly of gold arrays on sapphire substrates, easily fabricated dynamic template widths of 1 μm can be used to fabricate nanostructured arrays as small as 100 nm. In comparison, passive templating can only achieve feature sizes as small as 500 nm using the same template width. Such structures would have 125 times the volume of those accessible through dynamic templating. To further illustrate this point, Fig. 7 compares the expected minimum feature size of the assembled gold structures accessible for passive and dynamic templating as a function of the template width. For passive templating, calculations are based on a template-width-to-gold-film-thickness ratio of 50, the value needed to assemble a single structure. This ratio value is derived from the theoretical calculations of Dornel

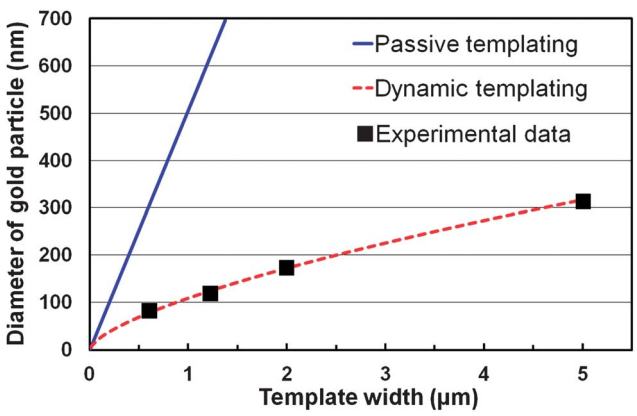

Fig. 7 Plot of the expected minimum gold nanoparticle diameter achievable on a sapphire substrate as a function of the template width for passive (solid) and dynamic templating (dashed). Also shown are the experimentally achieved values (squares) for the dynamic templating case. Note that dynamic templating has a significant advantage over passive templating regardless of the template width used.

et al.[44] utilizing the experimental gold-on-sapphire contact angle of 130°,[55] but is also consistent with our experimental findings. For the case of dynamic templating, the limitation of the assembly process is not the template-width-to-gold-film-thickness ratio, but the ability to maintain a quasi-continuous capping layer on the surface of the pedestal. With experiments indicating that capping layer integrity is maintained for a monolayer of gold for four different pedestal widths (0.6, 1.2, 2 and 5 μm), this monolayer value provides an appropriate choice for determining the expected minimum feature size. The calculation illustrates that dynamic templating is likely to have a significant advantage over passive templating on all length-scales. While shadow masks have been exclusively used in this study to form the dynamic template they are, by no means, a requirement of the assembly process as any conventional or unconventional lithographic process can be applied. Thus, the minimum feature size accessible through any of these individual lithographic techniques can be significantly improved upon through the formation and subsequent assembly of dynamic templates into much smaller structures. A further advantage is that nanostructures of varying sizes can be derived from the same lithographic pattern by simply varying the amount of gold placed on the antimony pedestals.

Conclusions

We have demonstrated a simple, inexpensive and versatile route for the templated dewetting of periodic arrays of sub-micrometer and nanoscale structures. Through the incorporation of a dynamic template into the conventional templated dewetting route, the assembly is no longer limited by the ratio of pattern-width-to-film-thickness. As a result, easily manufactured templates with micrometer-scale feature sizes are able to direct the assembly of nanometer-scale structures. Thus, with modest levels of instrumentation any reasonably equipped researcher is able to fabricate nanostructured arrays that would otherwise require advanced fabrication facilities. Nanostructures produced in this manner are well-spaced, providing an excellent platform for discovery in areas where arrayed nanostructures can be monitored as they (i) evolve into nanowires *via* the vapour–liquid–solid mechanism,[12] (ii) are used to initiate substrate-based templated assembly processes,[47,56] (iii) where they are sculpted into more intricate structures[57] or (iv) provide lab-on-a-chip functionalities.[58,59] In combination with more sophisticated lithographic techniques, able to define the dynamic template on smaller length-scales, there is also the strong likelihood that dynamic templates will be capable of producing dense arrays with nanostructure dimensions at or below those accessible to any individual lithographic process. Should this potential be realized, dynamic templating could emerge as a pervasive materials processing route.

Experimental methods

Gold array formation

Depositions were carried out at room temperature using a Neocera Pioneer 120 pulsed laser deposition system (Lambda Physik Compex 102 excimer laser, $\lambda = 248$ nm, laser energy density = 1.5 J cm^{-2}, laser spot size = 4 mm × 1.4 mm, laser repetition rate 10 Hz) where the thickness deposited per laser pulse was determined by calibrations based on AFM measurements. Most targets were derived from high purity metal foils (Alfa Aesar) which were cut to the 1″ diameter required. Exceptions were the germanium and antimony targets which were derived from a single crystal wafer (MTI) and a commercial supplier of targets (Kurt J. Lesker), respectively. Substrate materials were obtained from standard sources (MTI, Virginia Semiconductor, Valley Design, Graphene Supermarket). Most experiments were carried out using shadow masks consisting of electroformed nickel mesh (Precision Eforming) with 5 μm × 5 μm square openings and a repeat spacing of 12 μm. During deposition the mask was mechanically clamped to a substrate (typical dimensions 8 mm × 8 mm, diameter of exposed area = 5 mm) resting on a rare earth magnet. The role of the magnet was to ensure conformal contact between the shadow mask and substrate by attracting the nickel to the substrate surface. Denser arrayed structures, such as those shown in Fig. 4, utilized TEM grids (Quantifoil) as shadow masks. Conformal contact was obtained by (i) applying a thin layer of acetone to the substrate, (ii) placing the grid on the substrate and (iii) then allowing the acetone to dry. For this case, the capillary forces present during the drying process bring the two surfaces into intimate contact. Antimony pedestals with a height of 300 nm and 50 nm were deposited for 5 μm and 1.2 μm mask openings, respectively. This deposition was immediately followed by a gold layer deposition of the desired thickness. All depositions were carried out with a substrate–target distance of 8 cm and a base pressure of 10^{-7} torr. The procedure used to fabricate the 19 nm gold nanostructures shown in Fig. 5 differed in that a 4 nm thick film of silver was deposited between the gold and the antimony pedestal. The sub-monolayer gold thickness required to obtain these structures was achieved using the small quantities of material derived per laser pulse (approximately 1 monolayer per 200 pulses) when the laser energy density is reduced to values near the laser ablation threshold.

The assembly process was carried out in a tube furnace under a 100 sccm flow of ultra-high purity argon. During the assembly the substrate was placed in an alumina crucible. The heating regimen when utilizing antimony pedestals involved elevating the temperature to 600 °C (*i.e.* a temperature where antimony readily sublimates) in 9 min, where it was held for 30 min. It is noted that ramping the temperature quickly to 600 °C yielded the highest quality arrays, but where durations shorter than 9 min were not investigated due to the limitations of the instrumentation used. The temperature was then elevated to higher values to promote further agglomeration and to drive off the remaining antimony. In general, high temperatures (950–1050 °C) were used when the substrate was able to withstand high processing temperatures (*e.g.* oxide substrates). When lower temperatures were required to limit substrate degradation (*e.g.* graphene) or interactions between the substrate and assembling materials (*e.g.* silicon) the sample was heated to 750 °C, cooled to room temperature and then cycled to 750 °C a second time. The temperature cycling proved effective in

removing the antimony. The removal of both antimony and silver to form the 19 nm gold structures in Fig. 5 was carried out by ramping the structures to a temperature of 930 °C where it was held for 3 minutes. It is noted that the processing conditions used to derive nanostructures other than gold (*i.e.* those in Fig. 6) are summarized in the ESI (Table S1†).

Instrumentation

SEM images were obtained using a FEI Quanta 400 Environmental Scanning Electron Microscope operating in secondary electron mode. AFM images were obtained using a Veeco Multimode Atomic Force Microscope in tapping mode. EDS measurements were obtained using a JEOL JEM-1400 Transmission Electron Microscope. The extinction spectra were obtained using a Cary 5000 UV-Vis-NIR Spectrophotometer operating in transmission mode (aperture diameter = 1 mm, scan rate = 15 nm min^{-1}, increment = 0.5 nm). The Raman spectra of graphene was measured using Renishaw inVia Raman Microscope with an argon ion laser excitation source (λ = 514 nm, spot size = 1 μm).

Simulations and data analysis

Nanoparticle size distributions were obtained from SEM images processed using the ImageJ software. DDA simulations of the extinction efficiency were obtained using DDSCAT (Version 7.2)[49,50] where the simulated structure was first created using LAMMPS.[60] The structure simulated consisted of a truncated gold sphere (diameter = 110 nm) sharing a contact angle of 130° with a cylindrical sapphire substrate having a diameter of 300 nm and a thickness of 20 nm. The gold nanoparticle and sapphire substrate were represented by 74 376 and 194 315 dipoles, respectively, where the spacing between dipoles is 2 nm. The dielectric functions for gold and sapphire were taken from Johnson and Christy[61] and Palik,[62] respectively.

Acknowledgements

This work is partially funded by the NSF CAREER Award of SN (DMR-1053416). The authors acknowledge the expertise of Dr F. Monson (Technical Director, Center for Microanalysis, Imaging, Research and Training, West Chester University) and Dr H. Zhou (Materials Research Facility, Temple University). They also acknowledge access to facilities, expertise and support offered by Dr C. Kagan (Department of Chemistry, University of Pennsylvania), Dr S. Tyagi (Department of Physics, Drexel University) and Dr G. Baran (Department of Mechanical Engineering, Temple University). The authors also acknowledge the contributions of D. Gicuki, C. Decker, E. Wong and M. Figueroa. KDG and ZEE acknowledge support received through a Temple University Graduate Student Fellowship and an NSF NUE Award (EEC-1042071), respectively.

Notes and references

1 X. Huang, S. Neretina and M. A. El-Sayed, *Adv. Mater.*, 2009, **21**, 4880.
2 E. C. Dreaden, A. M. Alkilany, X. Huang, C. J. Murphy and M. A. El-Sayed, *Chem. Soc. Rev.*, 2012, **41**, 2740.
3 N. Liu, M. L. Tang, M. Hentschel, H. Giessen and A. P. Alivisatos, *Nat. Mater.*, 2011, **10**, 631.
4 H. Jans and Q. Huo, *Chem. Soc. Rev.*, 2012, **41**, 2849.
5 Y. Liu, R. Cheng, L. Liao, H. L. Zhou, J. W. Bai, G. Liu, L. X. Liu, Y. Huan and X. F. Duan, *Nat. Commun.*, 2011, **2**, 579.
6 H. A. Atwater and A. Polman, *Nat. Mater.*, 2010, **9**, 205.
7 J. A. Schuller, E. S. Barnard, W. Cai, Y. C. Jun, J. S. White and M. L. Brongersma, *Nat. Mater.*, 2010, **9**, 193.
8 N. C. Lindquist, P. Nagpal, K. M. McPeak, D. J. Norris and S.-H. Oh, *Rep. Prog. Phys.*, 2012, **75**, 036501.
9 B. D. Terris, *J. Magn. Magn. Mater.*, 2009, **321**, 512.
10 H. T. Chen, W. J. Padilla, J. M. O. Zide, A. C. Gossard, J. J. Taylor and F. D. Averitt, *Nature*, 2006, **444**, 597.
11 Z. Ma and S. Dai, *Nano Res.*, 2011, **4**, 3.
12 K. A. Dick, *Prog. Cryst. Growth Charact.*, 2008, **54**, 138.
13 R. R. Dammel, F. M. Houlihan, R. Sakamuri, D. Rentkiewicz and A. Romano, *J. Photopolym. Sci. Technol.*, 2004, **17**, 587.
14 T. Watanbe and H. Kinoshita, *J. Photopolym. Sci. Technol.*, 2008, **21**, 777.
15 C. Cheng and R. H. Lipson, *Laser Photonics Rev.*, 2010, **4**, 568.
16 C. G. Wilson, *J. Photopolym. Sci. Technol.*, 2009, **22**, 147.
17 J. A. Rogers and H. H. Lee, *Unconventional Nanopatterning Techniques and Applications*, John Wiley and Sons, Hoboken, New Jersey, 2009.
18 G. L. Jay, *Adv. Mater.*, 2007, **19**, 495.
19 Y. N. Xia and G. M. Whitesides, *Annu. Rev. Mater. Sci.*, 1998, **28**, 153.
20 K. Y. Suh, Y. S. Kim and H. H. Lee, *Adv. Mater.*, 2001, **13**, 1386.
21 C. L. Haynes and R. P. Van Duyne, *J. Phys. Chem. B*, 2001, **105**, 5599.
22 S. Aksu, A. A. Yanik, R. Adato, A. Artar, M. Huang and H. Altug, *Nano Lett.*, 2010, **10**, 2511.
23 O. Vazquez-Mena, T. Sannomiya, L. G. Villanueva, J. Voros and J. Brugger, *ACS Nano*, 2011, **5**, 844.
24 S. M. Seo, J. Y. Park and H. H. Lee, *Appl. Phys. Lett.*, 2005, **86**, 133114.
25 C. Wang, Q. F. Xia, W. D. Li, Z. L. Fu, K. J. Morton and S. Y. Chou, *Small*, 2010, **6**, 1242.
26 C. V. Thompson, *Annu. Rev. Mater. Res.*, 2012, **42**, 399.
27 F. Silly and M. R. Castell, *Phys. Rev. Lett.*, 2005, **4**, 046103.
28 C. Sönnichsen, B. M. Reinhard, J. Liphardt and A. P. Alivisatos, *Nat. Biotechnol.*, 2005, **6**, 741.
29 S. J. Henley, J. D. Carey and S. R. P. Silva, *Phys. Rev. B: Condens. Matter Mater. Phys.*, 2005, **72**, 195408.
30 C. Y. Hsu, J. W. Huang, S. Gwo and K. J. Lin, *Nanotechnology*, 2010, **21**, 035302.
31 C. M. Müller, F. C. F. Mornaghini and R. Spolenak, *Nanotechnology*, 2008, **19**, 485306.
32 G. A. Devenyi, J. F. Li, R. A. Hughes, A. C. Shi, P. Mascher and J. S. Preston, *Nano Lett.*, 2009, **9**, 4258.
33 J. Ye and C. V. Thompson, *Adv. Mater.*, 2011, **23**, 1567.
34 S. Curiotto, H. Chien, H. Meltzman, P. Wynblatt, G. S. Rohrer, W. D. Kaplan and D. Chatain, *Acta Mater.*, 2011, **59**, 5320.

35 S. Hajjar, G. Garreau, L. Josien, J. L. Bubendorff, D. Berling, A. Mehdaoui, C. Pirri, T. Maroutian, C. Renard, D. Bouchier, M. Petit, A. Spiesser, M. T. Dau, L. Michez, V. Le Thanh, T. O. Mentes, M. A. Nino and A. Locatelli, *Phys. Rev. B: Condens. Matter Mater. Phys.*, 2011, **84**, 125325.
36 F. Y. Lee, K. H. Fung, T. L. Tang, W. Y. Tam and C. T. Chan, *Curr. Appl. Phys.*, 2009, **9**, 820.
37 D. Kim, A. L. Giermann and C. V. Thompson, *Appl. Phys. Lett.*, 2009, **95**, 251903.
38 J. Ye and C. V. Thompson, *Phys. Rev. B: Condens. Matter Mater. Phys.*, 2010, **82**, 193408.
39 J. D. Fowlkes, L. Kondic, J. A. Diez, A. G. González, Y. Wu, N. A. Roberts, C. E. McCold and P. D. Rack, *Nanoscale*, 2012, **4**, 7376.
40 A. Sundar, C. J. Decker, R. A. Hughes and S. Neretina, *Mater. Lett.*, 2012, **76**, 155.
41 A. L. Giermann and C. V. Thompson, *J. Appl. Phys.*, 2011, **109**, 083520.
42 S. Yang, F. Xu, S. Ostendorp, G. Wilde, H. Zhao and Y. Lei, *Adv. Funct. Mater.*, 2011, **21**, 2446.
43 S. Hong, T. Kang, D. Choi, Y. Choi and L. P. Lee, *ACS Nano*, 2012, **6**, 5803.
44 E. Dornel, J. C. Barbe, F. de Crecy, G. Lacolle and J. Eymery, *Phys. Rev. B: Condens. Matter Mater. Phys.*, 2006, **73**, 115427.
45 A. Sundar, R. A. Hughes, P. Farzinpour, K. D. Gilroy, G. A. Devenyi, J. S. Preston and S. Neretina, *Appl. Phys. Lett.*, 2012, **100**, 013111.
46 W. R. Tyson, *Surf. Sci.*, 1977, **62**, 267.
47 M. R. Jones, K. D. Osberg, R. J. Macfarlane, M. R. Langille and C. A. Mirkin, *Chem. Rev.*, 2011, **111**, 3736.
48 J. Stadler, T. Schmid and R. Zenobi, *ACS Nano*, 2011, **5**, 8442.
49 B. T. Draine and P. J. Flatau, *J. Opt. Soc. Am. A*, 1994, **11**, 1491.
50 B. T. Draine and P. J. Flatau, *User Guide to the Discrete Dipole Approximation Code DDSCAT 7.2*, http://arXiv.org/abs/1202.3424, 2012.
51 P. Protsenko, J.-P. Garandet, R. Voytovych and N. Eustathopoulos, *Acta Mater.*, 2010, **58**, 6565.
52 O. Kozlova, R. Voytovvych, P. Prosenko and N. Eustathopoulos, *J. Mater. Sci.*, 2010, **45**, 2099.
53 L. Yin, B. T. Murray and T. J. Singler, *Acta Mater.*, 2006, **54**, 3561.
54 E. B. Webb III, G. S. Grest, D. R. Heine and J. J. Hoyt, *Acta Mater.*, 2005, **53**, 3163.
55 D. Chatain, F. Chabert, V. Ghetta and J. Fouletier, *J. Am. Ceram. Soc.*, 1993, **76**, 1568.
56 M. Grzelczak, J. Vermant, E. M. Furst and L. M. Liz-Marzan, *ACS Nano*, 2010, **4**, 3591.
57 C. J. Murphy, L. B. Thompson, D. J. Chernak, J. A. Yang, S. T. Sivapalan, S. P. Boulos, J. Y. Huang, A. M. Alkilany and P. N. Sisco, *Curr. Opin. Colloid Interface Sci.*, 2011, **16**, 128.
58 C. K. Dixit and A. Kaushik, *Biochem. Biophys. Res. Commun.*, 2012, **419**, 316.
59 W. H. Suh, Y. H. Suh and G. D. Stucky, *Nano Today*, 2009, **4**, 27.
60 S. Plimpton, *J. Comp. Physiol.*, 1995, **117**, 1, http://lammps.sandia.gov.
61 P. B. Johnson and R. W. Christy, *Phys. Rev. B: Condens. Matter Mater. Phys.*, 1972, **6**, 4370.
62 E. D. Palik, *Handbook of optical constants of solids*, Academic Press, San Diego, 1998.

